MODELING ULTRASONIC BEAM PROPAGATION IN GRAPHITE COMPOSITES

F. J. Margetan, B. P. Newberry, T. A. Gray,
and R. B. Thompson

Center for NDE
Iowa State University
Ames, IA 50011

INTRODUCTION

A continuing project at the Center for NDE in Ames involves the development of models which predict the probability of detecting flaws using a given inspection system.[1] Our general approach as it applies to through-transmission immersion inspections is as follows. With the two transducers to be used in the inspection, a reference experiment is performed to determine relevant information concerning equipment characteristics and transducer efficiencies. This may be done by placing a calibration specimen into the ultrasonic beam and measuring the time-domain electrical signal in the output cable of the receiver. Using models, we then predict how this received electrical signal would be changed if the calibration specimen were removed and unflawed and flawed components were placed into the beam in turn. The two components are assumed to have identical geometries except for a hypothetical flaw of given type, size, and orientation. If the difference between the predicted output signals for the two components is sufficiently large, compared to system noise, then the hypothetical flaw is said to be detectable.

Our specific approach for predicting output electrical signals and the approximations that we use are described in detail in Ref. 2. Briefly, we use Auld's reciprocity[3] formula to relate the electric fields in the cables to UT fields in the solid. A Gauss-Hermite (GH) beam model is used to describe the propagation of sound through water and through unflawed homogeneous material, and a Kirchhoff approximation is used to describe the scattering of sound by cracklike defects. We perform a series of calculations at discrete frequencies within the transducers' bandwidths, and we then combine these using an inverse Fourier transform to obtain the predicted time-domain output signal.

To validate our approach we obtained graphite/epoxy laminates with seeded delaminations from LTV Aerospace and Defense Company (Dallas, Texas). The laminated plates were approximately 0.8 cm thick, consisting of 64 layers of fiber-reinforced "pre-preg" tape. The layers were assembled in a quasi-isotropic fashion with fiber orientations of 0°, ±45°, and 90° equally represented. Using 10-MHz, planar, broadband transducers with beams oriented normal to the plate surfaces and the graphite fibers, we measured the signals received through flawed and unflawed portions of each plate. An analysis of these experiments indicated that the inherent anisotropy of the composite plates was not an important factor; the specimens were quasi-isotropic in structure and relatively thin, and the wavefronts entering the specimen were nearly

planar. As reported in Ref. 2, good agreement was found between measured and predicted time-domain flaw signals, when the plate was treated as an isotropic solid and the GH beam model was used. More recently, an extension of the GH model to anisotropic materials has been developed by R. B. Thompson and B. P. Newberry[4]. This paper describes preliminary experiments performed to evaluate this beam model for possible use in probability of detection (POD) applications.

EXPERIMENTS WITH FOCUSSED PROBES

Through-transmission inspections of plates are usually carried out with normally incident beams. Even at normal incidence obvious anisotropic effects can be readily observed when focussed probes are used to inspect anisotropic solids. For example, consider using a focussed transducer in water to inspect a plate of uniaxial graphite composite, with the transducer located very near to the plate. Two cross-sections of the inspecting beam are depicted in Fig. 1: on the left we view a plane parallel to the fiber direction (xz-plane), and on the right, a plane perpendicular to the fibers (yz-plane). For quasi-longitudinal waves propagating in the solid, the phase velocity is roughly three times greater along the fibers than it is perpendicular to them. Thus the local wavefronts entering the solid undergo the greater refraction in the xz plane. In addition, the skewing of energy propagation directions away from normal within the solid is greater in this plane. As a result of these two effects, the sound focusses earlier in the xz plane than it does in the yz plane. For a circularly symmetric transducer, the incident beam in water will possess rotational symmetry about its central (z) axis. However, this will not be true of the exiting beam in water. Depending on the frequency of the beam and on how far below the sample one looks, the emerging beam may be broader along the fiber direction, or broader in the direction perpendicular to the fibers.

We have carried out experiments to map the emerging sound field for the geometry suggested by Fig. 1. Our experimental arrangement is pictured in the upper left quadrant of Fig. 2. The uniaxial plate is submerged in water, and insonified by a focussed probe. We then use a "point probe" having a very small transducer element to receive the transmitted sound. The transmitter position is fixed, and the point probe is scanned in the x and y directions, i.e., parallel to the lower surface of the plate. (Here x will always denote the coordinate axis parallel to the fiber direction.) Partial results of one such C-scan are displayed in the other three quadrants of Fig. 2. On the vertical axis of each graph we display the magnitude of a selected frequency component in the Fourier spectrum of the received voltage pulse. In Fig. 2, the 2, 4, 6-MHz components of the received signal are displayed, each normalized to a value of unity at the center of the field. These figures may be regarded as maps of the particle displacement or pressure amplitude fields of the emerging beam at these frequencies.

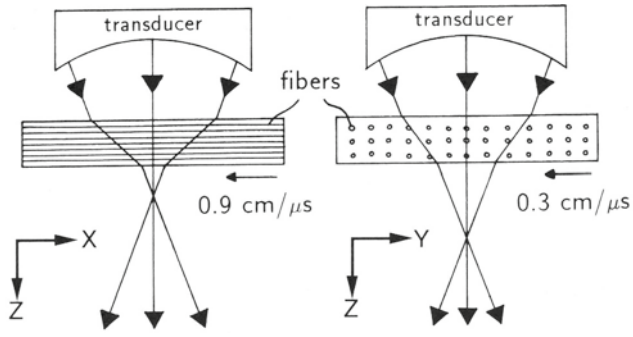

Fig. 1. Focussed beam incident upon a plate of uniaxial graphite composite: typical raypaths for energy propagation.

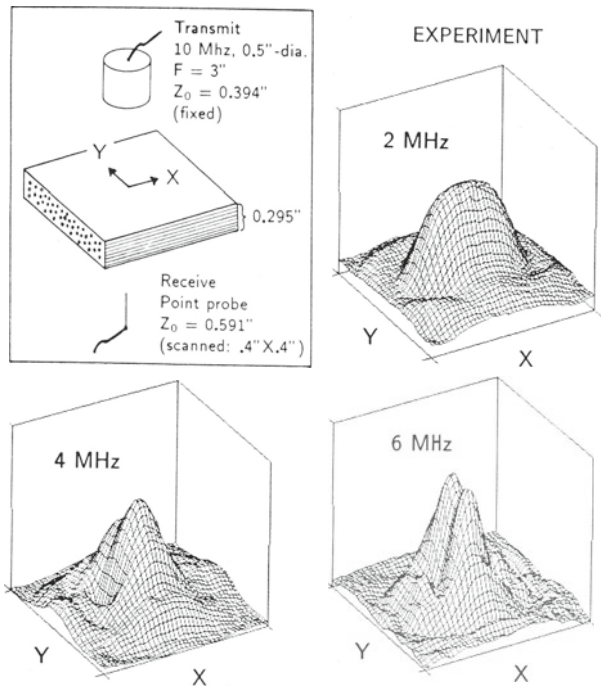

Fig. 2. Field mapping geometry (top left), and measured field amplitudes at 2, 4, and 6-MHz as functions of scan coordinates x and y.

For all of the experimental results reported in this work, the following points apply. The transmitter was a standard Panametrics circular immersion probe with a 0.5"=1.27 cm diameter and a 3"=7.62 cm focal length in water. The transmitter was a broadband probe having a center frequency of 10-MHz; however, the point probe was more sensitive at lower frequencies, and our most reproducible observations were made in the 1-6 MHz range. The point probe had an active diameter of $\lesssim$ 0.5 mm, and was fabricated by G. J. Posakony at Battelle Pacific NW. The plate of uniaxial graphite/epoxy composite was 0.75 cm thick, constructed of 64 layers of "pre-preg" tape (A5-4/3502) with all fibers directions aligned. Assuming full rotational symmetry about the fiber direction, speeds of longitudinal and transverse sound waves propagating along the x, y, and z axes were measured to determine the stiffness constants C_{11}, C_{22}, C_{44}, and C_{66}. The fifth independent constant, C_{12}, was then chosen to reproduce the off-diagonal Poisson's ratio $\nu_{12} = 0.31$ measured by LTV for the generic material. This resulted in:

$$\begin{aligned} &\text{Density} = 1.61 \ gm/cm^3 \\ &C_{11} = 139 \qquad C_{12} = C_{13} = 7.2 \qquad C_{22} = C_{33} = 15.6 \\ &C_{44} = 4.0 \qquad C_{55} = C_{66} = 7.4 \qquad C_{23} = C_{22} - 2C_{44} = 7.6 \quad (\text{in} GPa) \end{aligned} \tag{1}$$

The vertical waterpaths in Fig. 2 were 0.39"=1.0 cm and 0.59"=1.5 cm on the top (transmitting) and bottom (receiving) sides of the plate, respectively. These values were chosen to enhance the asymmetry of the resulting field patterns. Beam asymmetry is clearly visible in the field maps displayed in Fig. 2. In the 2-MHz field profile, the central lobe is about twice as wide in the x-dimension (parallel to the fibers) as it is in the y-dimension. At 4-MHz, the situation is reversed, with the beam now narrower along the fiber direction. At 6-MHz, an interesting beam profile is observed: along the fiber direction, the beam has a narrow central lobe and prominent shoulders; perpendicular to the fibers there is a broad central lobe with a pronounced depression at its center.

COMPARISON WITH THEORY

POD studies require a beam model that is both reasonably accurate and rapid to compute. One candidate is the GH model, and a brief outline of its development appears below. Here we confine the theory to the case of beam propagation along a principal axis of the solid. Further details of the model development and treatments of more general cases can be found in Ref. 4.

We assume a homogeneous, linear, anisotropic solid, and consider an ultrasonic beam propagating in the z-direction through this solid. For a given angular frequency ($\omega = 2\pi f$) and wavetype (e.g., quasi-longitudinal) we write the particle displacement field as an angular spectrum of plane waves:

$$U(x,y,z)e^{i\omega t} = \frac{1}{4\pi^2}\int_{-\infty}^{\infty}\int_{-\infty}^{\infty} dk_x dk_y \phi(k_x,k_y)e^{i(\omega t - \vec{k}\cdot\vec{r})} \qquad (2)$$

Here $\omega/|\vec{k}|$ is the phase propagation speed for the plane wave propagating in direction $\vec{k}$. We assume that the various plane waves that contribute strongly in Eq. (2) have similar polarization vectors; thus the polarization direction is fixed and does not appear explicitly. For each plane wave, the z-component of the wave vector is determined by the x and y-components and the phase velocity, the phase velocity in a given direction being determined by the wave type and the elastic constants of the solid. In the exponent of Eq. (2) we make a Fresnel approximation, i.e., we write k_z as a quadratic function of k_x and k_y. In other words, we approximate the exact slowness surface in the forward direction by a paraboloid:

$$\left(\frac{k_z}{\omega}\right) \approx \left(\frac{k_z}{\omega}\right)_{para.} = S_0 + \left(C_x - \frac{1}{2S_0}\right)\left(\frac{k_x}{\omega}\right)^2 + \left(C_y - \frac{1}{2S_0}\right)\left(\frac{k_y}{\omega}\right)^2 \qquad (3)$$

Here S_0 is the slowness (i.e. the inverse of the phase speed) for plane waves propagating in the forward (z) direction. The terms $1/(2S_0)$ have been included for convenience; they insure that for an isotropic solid the curvature parameters take the values $C_x = C_y = 0$ when Eq. (3) is obtained from a Taylor's series expansion of the exact slowness surface. The plane wave amplitude function, $\phi(k_x,k_y)$, can be written as a two-dimensional spatial Fourier transform of the displacement field on some initial plane. We then write this initial field as a sum of Gauss-Hermite functions, i.e., Gaussians times Hermite polynomials:

$$\phi(k_x,k_y) = \int_{-\infty}^{\infty}\int_{-\infty}^{\infty} dx dy U(x,y,0)e^{i(k_x x + k_y y)} \qquad (4)$$

$$U(x,y,0) = \sum_{m,n} A_{mn} e^{-\alpha x^2} H_m(\sqrt{2Re(\alpha)}x) e^{-\alpha' y^2} H_n(\sqrt{2Re(\alpha')}y) \qquad (5)$$

Eqs. (3)-(5) are then substituted into Eq. (2). The resulting integrals can be performed analytically, and we are left with an expression for $U(x,y,z)$ as a sum of GH functions, similar to Eq. (5). Now, however, the complex parameters α and α' (which describe the widths and radii of phase curvature of the expansion functions), depend on the propagation distance z. In fact, simple rules can be found which describe how these parameters change as the beam propagates through space or traverses an interface. In practice, the A_{mn} are evaluated at the face of the transmitting transducer by using orthogonality properties of the GH functions. We then propagate the expansion functions (i.e. propagate the α and α') through the various layers of material to the receiving plane, where the field is evaluated.

As described above, the GH beam model approximates a local region of a material's slowness surface with a paraboloid. In Fig. 3, we display two cross-sections of the quasi-longitudinal slowness surface for our graphite composite, as determined from the elastic constants of

Eq. (1). The radial distance from the origin to the surface along a given direction specifies the inverse phase speed (slowness) for plane waves propagating in that direction. Along the fiber direction (x), the wave speed is high, and hence the slowness is small. In the plane perpendicular to the fibers (yz), the wave speed is independent of direction and the slowness curve is a circle. In the experiments previously described, the focussed beam was aligned with z-axis. Thus we must approximate the upper portions of the slowness curves in Fig. 3 with parabolas. An expanded view of the region of interest in the xz plane is shown in Fig. 4. There the solid curve is the actual slowness function, and the other two curves are parabolic approximations to it. The region shown covers plane waves propagating in directions within 14° of the z-axis. In the usual application of the Fresnel approximation, one makes a Taylor's series expansion of the slowness surface about the forward direction. This leads to the dotted parabola in Fig. 4 ($C_x = -0.18 cm/\mu s$) which has the same intercept and curvature at $k_x/\omega = 0$ as the actual slowness curve. Such a parabola would be appropriate for a well-collimated beam propagating in the z direction. However, in our experiments we have used a focussed probe which emits sound over a range of angles. By examining the angular distribution of plane waves comprising the beam, one can determine which propagation directions contribute significantly. For our transducer we find appreciable plane wave strength out to 5° or 6° from forward in the water, and hence out to 12° or 15° from forward in the xz plane of the solid. This suggests that we approximate the actual slowness surface with a sharper parabola, like the dashed curve in Fig. 4 ($C_x = -0.4 cm/\mu s$) which provides an "average" fit over the region shown. One can perform a similar analysis in the yz plane; there one finds that the Taylor's parabola ($C_y = 0$) is also a good "average" parabola for the slowness region of interest.

Because the curvature of the paraboloid determines the diffraction of the propagating beam, the choice of curvature can strongly influence the emerging fields predicted by the GH model. For the geometry of Fig. 2, Fig. 5 compares the measured 6-MHz displacement field with three fields predicted by the GH model. The field in the upper right quadrant results from treating the composite plate as an <u>isotropic</u> solid ($C_x = C_y = 0$); it has full rotational symmetry and a deep central depression. The <u>anisotropic</u> model treatments using the Taylor's paraboloid ($C_x = -0.18 cm/\mu s, C_y = 0$) and the "average" paraboloid ($C_x = -0.4 cm/\mu s, C_y = 0$) appear in the lower half of Fig. 5. The degree of

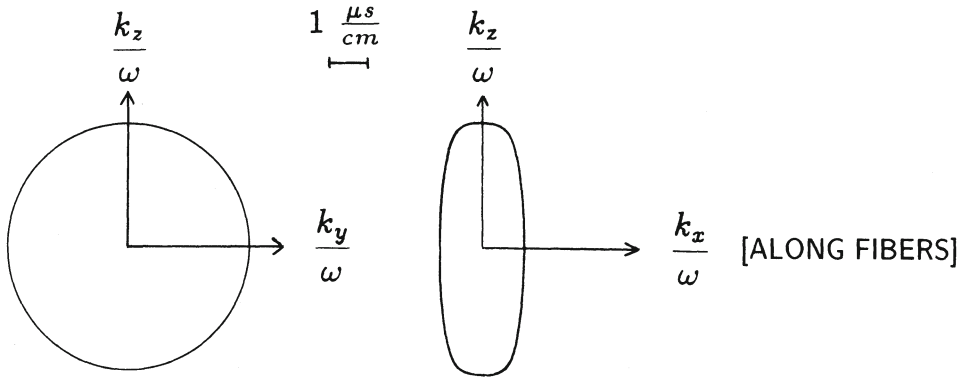

Fig. 3. Quasi-longitudinal slowness surface cross-sections for the uniaxial composite specimen. Fibers are parallel to the x-axis.

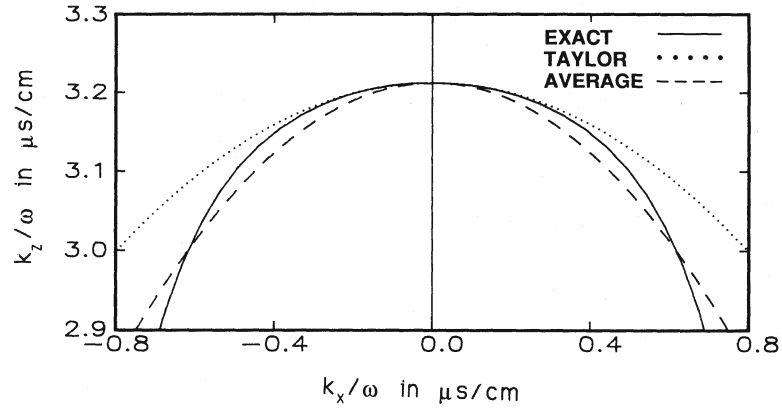

Fig. 4. Detail of the slowness curve in the xz plane and two parabolic approximations to it.

agreement between model and experiment can be better gauged by viewing slices of these field maps, as in Fig. 6. The 6-MHz experimental values shown in Fig. 6 result from six scans of the point probe through the center of the emerging beam using different portions of the plate. Three scans were made parallel to the fiber direction, and three perpendicular to it. Data to the left and right of center were then "folded over" to further average and symmetrize the results. For each frequency component, all experimental and anisotropic model fields have been normalized to unity at x=y=0. In the direction perpendicular to the fibers both anisotropic model predictions agree well with the 6-MHz experimental data; however, parallel to the fibers, the "average" paraboloid does much better with good reproduction of the central lobe and the first shoulder. Similar comparisons of model predictions and experimental data for 2 and 4 MHz are displayed in Fig. 7.

SUMMARY AND DISCUSSION

Using a focussed source and small diameter receiver, we have mapped the ultrasonic field transmitted through a submerged plate of uniaxial graphite composite. Waterpaths were chosen to emphasize anisotropic effects. Experimental results were then compared to the predictions of a GH beam model for homogeneous anisotropic solids. One model approximation is the replacement of the solid's slowness surface by a paraboloid, and good agreement between theory and experiment was found when the paraboloid was properly chosen.

When applying the GH beam model to new situations, it will be helpful to have an algorithm for estimating an optimal slowness parabola, e.g., for estimating optimal values of C_x and C_y in Eq. (3). Recall that in the development of the GH model we wrote the particle displacement field as an angular spectrum of plane waves, and we tacitly assumed that the exact (k_z/ω) and approximate $(k_z/\omega)_{para}$ slowness components were similar whenever the plane wave amplitude function, $\phi(k_x, k_y)$, was large. This suggests choosing the slowness parabola by minimizing the difference between the two k_z/ω values using $\phi(k_x, k_y)$ as a weighting function. Consider, for example, wave propagation in the xz plane of the composite. One could choose C_x to minimize

$$\int_{-\infty}^{\infty} dk_x \, |\phi(k_x, 0)|^{p_1} \left| \frac{k_z}{\omega} - \left(\frac{k_z}{\omega} \right)_{para} \right|^{p_2}$$

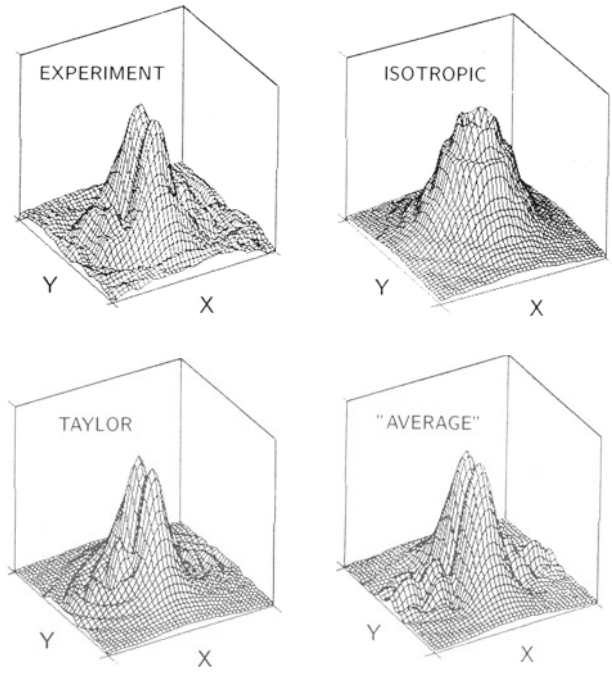

Fig. 5. Measured 6-MHz field pattern, and predicted displacement field amplitudes using three versions of the Gauss-Hermite model.

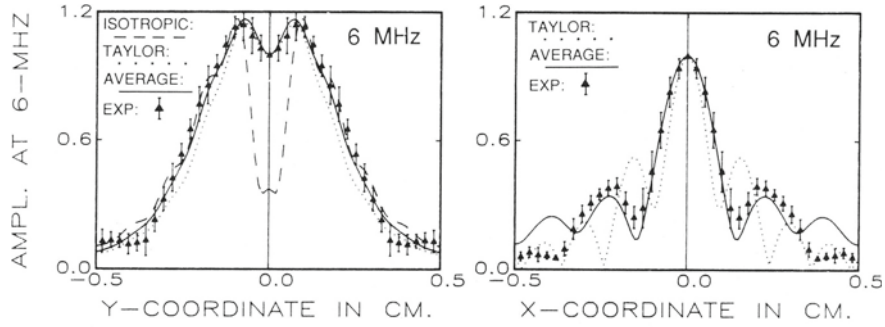

Fig. 6. Measured and predicted amplitudes at 6-MHz for the geometry of Fig. 2.

where $(k_z/\omega)_{para}$ is a function of C_x given by Eq. (3) with $(k_y/\omega) = 0$, and where p_1 and p_2 are weighting powers available for tuning the algorithm as experience in its use is accumulated. C_y could be similarly determined by a minimization in the yz plane. The suggested minimization procedure has been carried out numerically for our probe/plate geometry and results appear in the right hand portion of Table 1 for $p_1 = p_2 = 1$. In the "EXP" column we list the ranges of C_x and C_y values which led to the best agreement with experiment, and in the "TAYLOR" column we list the curvature parameters resulting from a Taylor's series expansion of the exact slowness surface about $k_x/\omega = k_y/\omega = 0$. The amplitude function $\phi(k_x, k_y)$ is different at different frequencies, and the minimization algorithm has been applied at 2, 4, and 6 MHz. Although further testing of the algorithm is in order, it appears to generate a better paraboloid estimation than does the Taylor's expansion.

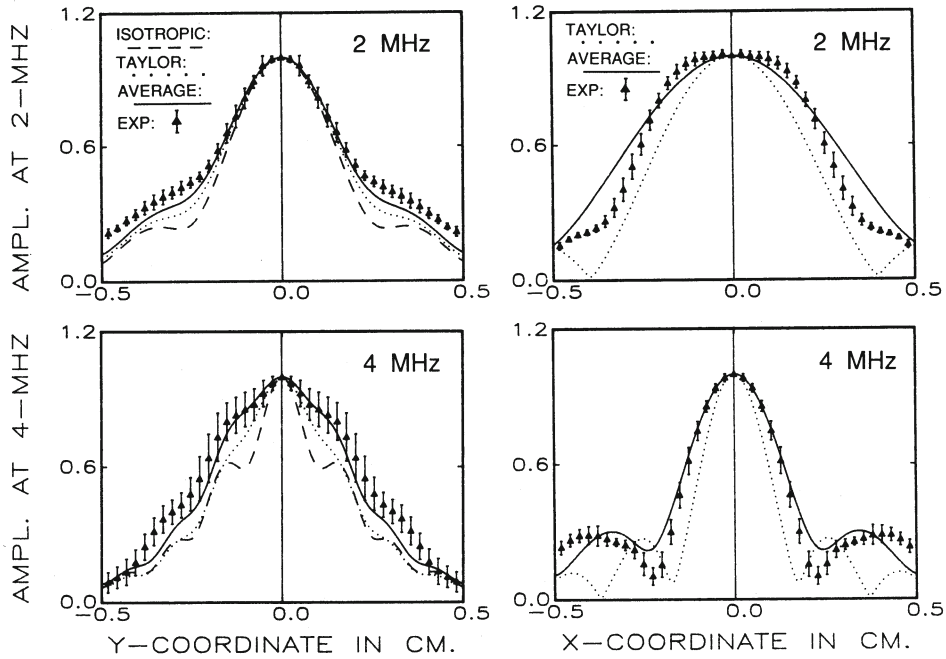

Fig. 7. Measured and predicted amplitudes at 2 and 4 MHz.

Table I. Paraboloid curvature parameters in $cm/\mu s$.

	"EXP"	Taylor	Algorithm 2-MHz	4-MHz	6-MHz
C_x	-0.4 ± 0.1	-0.18	-0.51	-0.43	-0.38
C_y	0 ± .02	0	-0.017	-0.015	-0.013

ACKNOWLEDGMENT

This work was sponsored by the Center for NDE at Iowa State University and was performed at the Ames Laboratory. Ames Laboratory is operated for the U.S. Department of Energy by Iowa State University under Contract No. W-7405-ENG-82. The authors wish to thank Ali Minachi and Ronald A. Roberts for supplying water/composite transmission coefficients.

REFERENCES

1. T. A. Gray, F. Amin, and R. B. Thompson, Review of Progress in QNDE 7B, D. O. Thompson and D. E. Chimenti, Eds., (Plenum Press, New York, 1988), p. 1737.
2. F. J. Margetan, T. A. Gray, R. B. Thompson, and B. P. Newberry, Review of Progress in QNDE 7B, D. O. Thompson, and D. E. Chimenti, Eds., (Plenum Press, New York, 1988), p. 1083.
3. B. A. Auld, Wave Motion 1 (1979), p. 3.
4. B. P. Newberry and R. B. Thompson, A paraxial theory for the propagation of ultrasonic beams in anisotropic solids, submitted to J. Acoust. Soc. Am.